Applied Magnetic Resonance (2021) 52:33–45
https://doi.org/10.1007/s00723-020-01220-2

Applied
Magnetic Resonance

ORIGINAL PAPER

# Synthesis, Characterization and MRI Application of Cobalt-Zinc Ferrite Nanoparticles Coated with DMSA: An In-vivo Study

**Leyla Ansari[1] · Ibrahim Sharifi[2] · Hadis Ghadrijan[3] · Negar Azarpira[4,5] · Farideh Momeni[1] · Hamed Zamani[6] · Naser Rasouli[3] · Mahdi Mohammadi[7] · Alireza Mehdizadeh[1,8] · Razzagh Abedi-Firouzjah[9]**

Received: 29 May 2020 / Revised: 11 July 2020 / Published online: 10 August 2020


**Abstract**
The aim of this study was to synthesize and characterize the dimercaptosuccinic acid (DMSA) cobalt–zinc (Co–Zn) ferrite magnetic nanoparticles (NPs) and their efficiency as a contrast agent in in vivo MR imaging of rat liver. Co–Zn ferrite NPs were synthesized by the thermal decomposition method and stabilized by DMSA. The NPs were characterized by different analyses to study their physical and magnetic properties and were injected into 6 adult male rats. Liver MRI was performed to measure the signal intensity at different times. The average nanoparticle size was estimated at about $8 \pm 1$ nm using transmission electron microscopy (TEM). The $r_2$ and $r_2$* relaxivity of these particles were obtained at 32.85 and 168.96 mmol $L^{-1}$ $s^{-1}$, respectively, using an agarose phantom imaged by MRI. In the in vivo condition, injection of SNPs (2.5 mg Fe/kg) showed negative contrast in a way that for $T_2$ and $T_2$* weighted the maximum contrast enhancement was 58.46 and 77.13%, respectively. Regarding our results, the synthesized Co–Zn ferrite NPs stabilized by DMSA are appropriate agents for increasing the contrast in both $T_2$ and $T_2$* weighted based on MR imaging in rat liver.

## 1 Introduction

Magnetic resonance imaging (MRI) has been a powerful technology as a diagnostic method for in vivo assessment of diseases with high resolution [1]. Enhancing the tissue contrast of the images obtained from this technique by adding extrinsic agents has become the necessary process for lots of patients. Magnetic NPs are widely used as

✉ Alireza Mehdizadeh
mehdizade@sums.ac.ir

✉ Razzagh Abedi-Firouzjah
razzaghabedi@gmail.com

Extended author information available on the last page of the article

contrast agents in MRI of liver and lymph node [2–4]. These contrast agents consist of magnetite ($Fe_3O_4$), maghemite ($\gamma Fe_2O_3$), ferrites ($MFe_2O_4$: $M$ = Co, Cu, Zn, Mn), manganese oxide, and other compounds, such as gadolinium complexes [5–8]. Frequently, superparamagnetic nanoparticles (SNPs) are used due to their negative enhancement effect on $T_2$- and $T_2^*$-weighted pulse sequences [9, 10].

Ferrite nanoparticles (NPs) as MRI contrast agents are providing several advantages over gadolinium-based contrast agents. Toxicity is considerably reduced due to biodegradability and detectability is greatly improved as they contain a high payload of contrast-generating agents [11, 12].

SNPs align with the external magnetic field and induce strongly localized magnetizations within tissues by interaction with surrounding water protons. The mode of action of ferrite NPs occurs by enhancing the relaxivity or shortening the $T_2$ relaxation time by increasing field inhomogeneity of surrounding protons to create strong negative MRI contrast [11]. The negative contrast enhancement of the NPs is directly proportional to the magnetic moments of the NPs. The effectiveness of the contrast agents is determined by different parameters, such as the size of the particles, charge, topographies of the coating, and hydrodynamic [13]. These physicochemical characteristics have an effect on stability, bio-distribution, opsonization, metabolism, as well as to their clearance from the vascular system [13, 14].

Co–Zn ferrite NP is one of the SNPs which has been the subject of several researchers as MRI contrast agents [15–17]. However, the previous studies focused on synthesis methods and applying these particles in cell lines. The contrast efficiency of these NPs has rarely been evaluated in in vivo conditions; thus, it needs more investigations.

MRI of the liver with NP contrast agents is an appropriate diagnostic method for assessing several diseases like liver cancer [18]. On the other hand, choosing an appropriate NP surface coating as a contrast agent is important and complex [14]. In this regard, there have been several studies evaluating NPs with different coating materials [19–22]. We used dimercaptosuccinic acid (DMSA) coating due to its hydrophilic properties in MRI applications, and also there are several reports about the non-toxicity property of this coating material in different cell lines [12, 19, 22].

Thus, in this study, DMSA-coated Co–Zn ferrite NPs ($Co_{0.6}Zn_{0.4}Fe_2O_4$) were synthesized by the thermal decomposition method. The physical characteristics and morphology of the NPs were investigated by TEM (transmission electron microscopy), XRD (X-ray diffraction), and FTIR (Fourier-Transform Infrared). The magnetic properties of NPs were obtained using a vibrating sample magnetometer (VSM). Then, the efficiency of contrast agents was obtained by the relaxivity of $r_2$, and $r_2^*$ using a 1.5-T MRI scanner. Finally, the usefulness of the NPs as a contrast agent in the rat liver was investigated.

## 2 Materials and Methods

### 2.1 Synthesis of Zinc–Cobalt Ferrite NPs

The thermal decomposition method as described by Sharifi et al. [23] was applied to synthesize the SPNs. Briefly, metallic acetylacetonate consisting of Fe $(acac)_3$

(2 mmol), Co $(acac)_2$ (0.6 mmol), Zn $(acac)_2$ (0.4 mmol) and stearyl alcohol (15 mmol) was added to a 3-necked balloon. A reactor was used for synthesizing SPNs, then 10 ml of benzyl ether and 30 ml oleylamine were added to the reactor. The reactor temperature increased to 60 ℃ for solving precursors. In the next step, the reactor was vacuumed for 15 min to empty the reactor system from oxygen and inject nitrogen gas as inert atmosphere. Afterwards, it was vacuumed again at 100 ℃ for 2 min. Finally, the temperature reached 330 ℃ in inert atmosphere and the mixture was refluxed for 30 min. After cooling to room temperature, the produced NPs were separated with magnetic field after several washing procedures with ethanol. A small number of NPs were dried for analysis and the remnant was dispersed into hexane due to hydrophobic characteristics of these NPs.

### 2.2 Surface Modification

The NPs must have hydrophilic properties in MRI applications; therefore, the NPs were functionalized with DMSA. The NPs were separated by adding alcohol for the purpose of suspension and centrifuging. 25 ml of toluene was mixed with 90 mg of DMSA in 5 ml of dimethyl sulfoxide (DMSO). Then, the obtained mixture was added to 50 mg of ferrite NPs. The mixture was solicited for five temperatures. The functionalized hydrophilic NPs were washed for several minutes and stirred for 24 h at room temperature with ethanol, then dispersed in water. A pH value of suspension was increased to 12 to have a good dispersion of NPs, which was then reduced to seven and dialyzed for 3 days.

### 2.3 Characterization and Cytotoxicity of the Nanoparticles

The phase purity of the obtained NPs was examined using a Philips X-ray diffractometer with Co-$K_\alpha$ radiation ($\lambda = 1.78901$ Å). Infrared absorption spectra of the naked and coated NPs were achieved by an FTIR system (Perkin-Elmer, 1403 spectrometer) in wavenumbers ranging between 400 and 4000 $cm^{-1}$. The morphology of the particles was measured using CM30 Philips TEM at 150 kV and the magnetization was measured by a VSM (Meghnatis Daghigh Kavir Co., Kashan, Iran) at room temperature.

The cytotoxicity of Co–Zn ferrite NPs was widely evaluated and described in previous studies for various concentrations [12, 22, 24, 25]. The concentration used in this study (2.5 mg/kg body weight), is much lower than the cytotoxic concentration in previous reports [12, 22, 24]; therefore, the cytotoxicity test was not performed in this study. The toxic effect of Co–Zn ferrite NPs coated with DMSA was also been evaluated in previous investigations [12, 19, 22], which showed high biocompatibility and non-toxic effects.

### 2.4 Phantom Study

An agarose phantom was utilized to access the efficacy of DMSA-coated SPIONs (Superparamagnetic iron oxide nanoparticles) as an MRI contrast agent, and for

measuring the relaxivity values, $r_2$ and $r_2$*. DMSA-coated SPIONs were solicited for 10 min, and different concentrations of SPIONs were prepared with agarose gel (1% W/V). The prepared concentrations were moved into a 96-well ELISA plate.

The phantom was scanned with a 1.5-T MRI (Magnetom Avanto, Siemens, USA) using a knee coil. $T_2$-weighted images [field of view (FOV) = 160 × 160 $mm^2$ with the slice thickness of 3 mm, time of repetition)TR(= 2700 ms, time of echo (TE) = 8 different time ranging from 15 to 88 ms, matrix = 230 × 256, flip angle (FA) = 150, and average = 2] and $T_2$*-weighted imaging (FOV = 499 × 499 $mm^2$ with the slice thickness of 4.5 mm, TR = 400 ms, TE = 8 different time ranging from 10 to 39 ms, matrix = 256 × 192, FA = 20, and average = 1) were obtained using spin-echo pulse sequence. The values of $r_2$ and $r_2^*$ were calculated by the curve fitting of plots of $1/T_2$ and $1/T_2^*$ (in $s^{-1}$) versus the sum of the concentration (in mmol $L^{-1}$).

### 2.5 In vivo Study

Six normal male rats with average weight (210–280 g) were studied to evaluate the constructed DMSA-coated SPIONs as MRI contrast agents in in vivo conditions. The study was approved by the Ethics Committee of Shiraz University of Medical Sciences.

The animals were scanned using a 1.5-T MRI machine. The fast spin-echo sequence with the scan parameters TR = 2700 ms, TE = 88 ms, FOV = 449 × 449 $mm^2$; slice thickness = 4.5 mm, matrix = 384 × 288, and FA = 150 for $T_2$, and TR = 395 ms, TE = 15 ms, FOV = 449 × 449 $mm^2$; slice thickness = 4.5 mm, matrix = 384 × 288, and FA = 30 for $T_2$* weighted was used to obtain the images.

The animals were anesthetized using ketamine (70 mg/kg) and xylazine (5 mg/kg). The DMSA–SPIONs were injected through the tail vein at a dose of 2.5 mg/ml of Fe/kg body weight. MRI scans were performed before injection and at 30, 38, 75 min, and 2 h afterwards. Signal intensities in rat liver were measured before and after the administration of DMSA–SPIONs.

## 3 Results

### 3.1 Magnetic and Structural Properties

Figure 1 shows the XRD pattern of Co–Zn ferrite NPs crystalline structure. The presence of a pure spinel phase was observed with the lattice parameter ($a$ = 8.423 Å) which was in good agreement with Jnaneshwara et al. study about the $Co_{0.6}Zn_{0.4}Fe_2O_4$ lattice constant (26). The Rietveld refinement analysis confirmed the crystallite NP average size, equal to 6.7 nm.

Infrared spectra of particles showed a broad band centered around 3400 $cm^{-1}$ probably due to symmetric ($\nu_s$) stretching vibrations of the amine groups of the oleylamine molecule. The twin bands were seen about 2921 $cm^{-1}$ showing stretching vibrations related to methylene groups. Also, bands around 1600 and 1380 $cm^{-1}$ are related to asymmetric and symmetric stretching modes of the

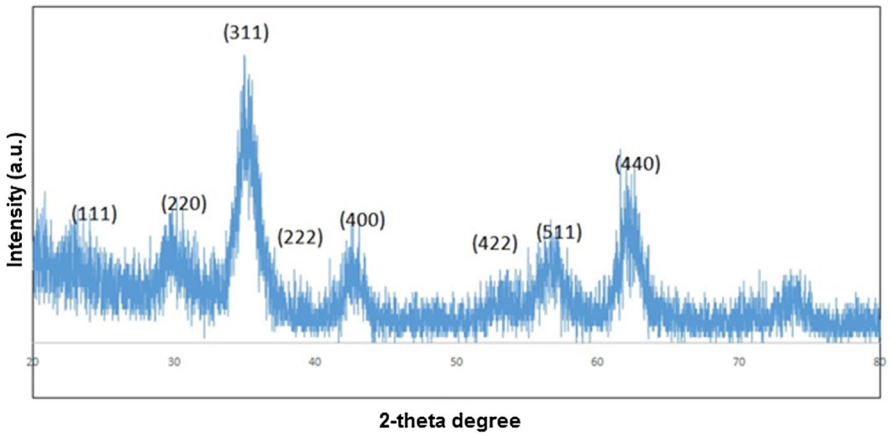


**Fig. 1** XRD pattern of cobalt-zinc nanoparticles

carboxylate groups, while bands about ~ 1100 $cm^{-1}$ arise from the S–CH bonds. Overall, peaks at 900, 1100, 1380, and 1600 $cm^{-1}$ presented in (Fig. 2) showed the DMSA coated on the magnetic NP surfaces. Moreover, peaks below 700 $cm^{-1}$ indicated the vibrational modes of the structure of the NPs. The two modes including $\nu_1$ (~ 586) and $\nu_2$ (~ 404) are the results of the stretching vibration of the tetrahedral and octahedral sites, respectively.

The SNIPs' magnetic behavior at room temperature is illustrated in (Fig. 3). The reversible and unsaturated form of the M–H curve, with a very low magnetic coactivity, confirmed that the NPs are superparamagnetic at room temperature. The maximum magnetization of NPs reached 34/3 $Am^2/kg$ around nine kOe (kilo Oersted) auxiliary magnetic field.

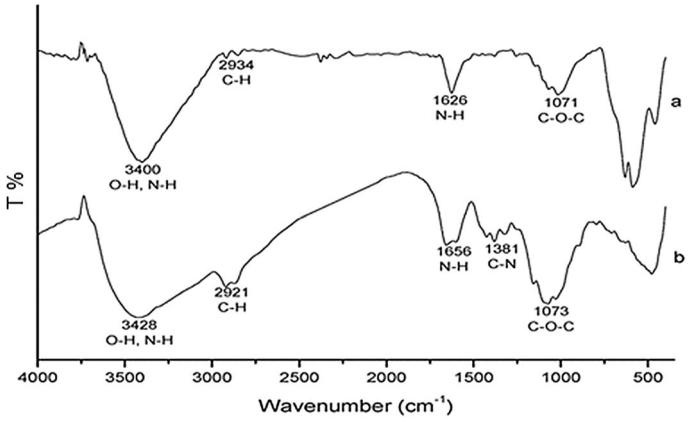


**Fig. 2** FTIR analysis of (**a**) uncoated and (**b**) coated magnetic nanoparticles

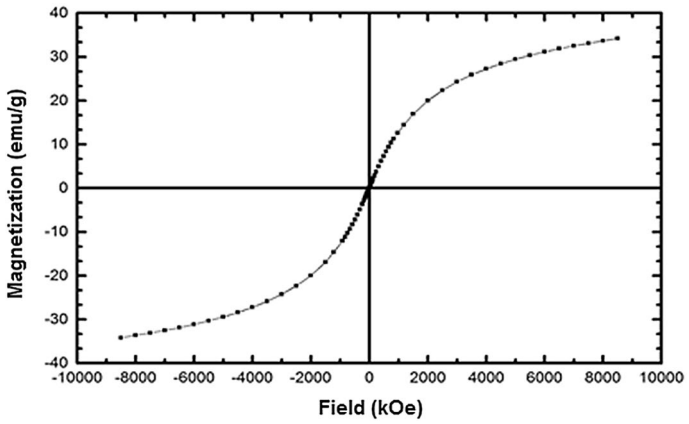


**Fig. 3** M-H curve of uncoated magnetic nanoparticles

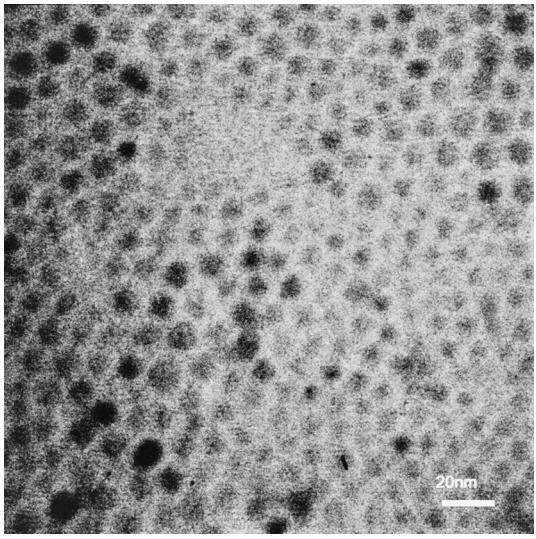


**Fig. 4** TEM micrograph of nanoparticles

The TEM image of the Co–Zn ferrite NPs is presented in (Fig. 4). As shown in the picture, the NPs are relatively uniform, spherical, and well separated from each other. Furthermore, there is no evidence of agglomeration in the particles. The particle size was estimated at about $9 \pm b2$ nm using SemAfore software (version 5.1, Insinooritoimisto Rimppi Oy, Finland).

### 3.2 Phantom Study

In Fig. 5, the demonstrations of the $T_2$ (TR = 2700 ms, TE = 66 ms)- and $T_2$* (TR = 400 ms, TE = 10 ms)-weighted images at different concentrations of NPs

are shown. The signal intensity of $T_2$- and $T_2^*$-weighted images was enhanced by decreasing the NPs' concentration.

The relaxivity ($r_2$ and $r_2^*$) of DMSA–SPIONs was measured to evaluate the potential use of DMSA-coated SPIONs as $T_2$- and $T_2$*-contrast agents in MRI examinations. There was a linear correlation between the relaxivities and concentration of the NPs. The relaxivity values of $r_2$ and $r_2$* obtained as 32.85 and 168.96 mmol $L^{-1}$ $s^{-1}$, respectively.

### 3.3 In vivo Studies

The liver uptake potential and efficiency of the DMSA–SPIONs were obtained by MR imaging of rat liver. Pre- and post-contrast $T_2$- and $T_2$*-weighted coronal images of the animals' livers are shown in (Figs. 6, 7), respectively. According to the figures, the average number of the highest variation in signal intensity for $T_2$-weighted images among the pre- and post-injection is $174.36 \pm 21.04$ and $72.44 \pm 17.36$, respectively. In the same way, for $T_2$*-weighted images, this number is $274.68 \pm 30.77$ for pre-contrast and $62.8 \pm 26.62$ for post-contrast images.

Regarding the results, the greatest variation (reduction) of signal intensity or contrast enhancement between the control and post-contrast groups for $T_2$ weighted was 58.46%, and 77.13% for $T_2$* weighted occurred about 30 and 120 min after injection, respectively.

## 4 Discussion

The Co–Zn ferrite NPs ($Co_{0.6}Zn_{0.4}Fe_2O_4$) were synthesized with and without DMSA coating. Furthermore, the physical characteristics of the constructed NPs were investigated to ascertain the penetration of these NPs to cells in in vivo conditions as well as the superparamagnetivity of these particles.

Overall, SPNs with the diameters above the 10 nm cannot be transferred across the vessels in a physiologically healthy non-inflammatory environment. In addition, the saturation magnetization can be reduced by decreasing the size of the NPs. This phenomenon has an unfavorable effect on magnetic properties. Also, if the size of the magnetic NPs was below 5.5 nm, these were quickly removed through renal clearance [26]. Therefore, one of the aims of this study was to produce the SNPs with a diameter ranging from 5.5 to 10 nm.

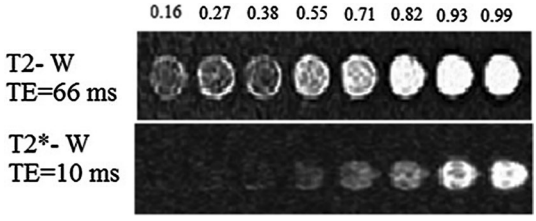


**Fig. 5** $T_2$ and $T_2^*$ weighted images of DMSA-coated magnetic NPs obtained from the phantom at different concentration (mmol $L^{-1}$)

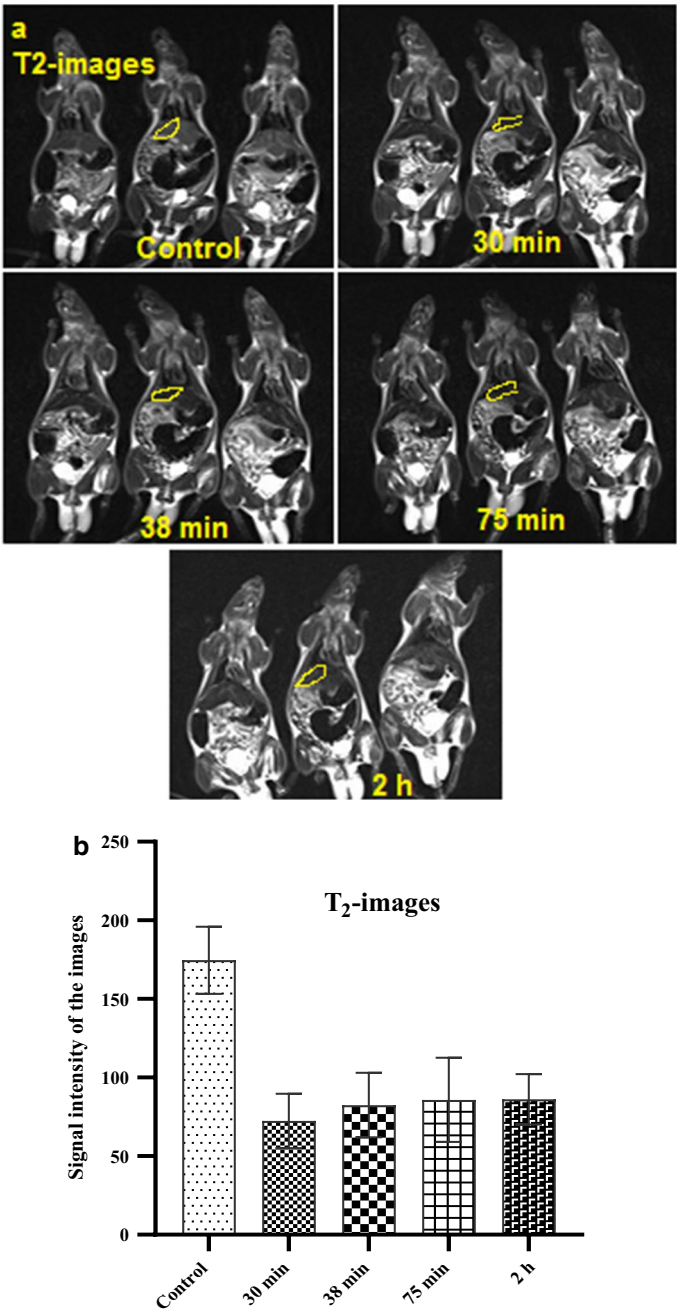


**Fig. 6** **a** *T2*-weighted MRI of the rat liver injected with DMSA-coated Zn-Co NPs; (**b**) signal intensity analysis for *T2*-weighted MR images at different time

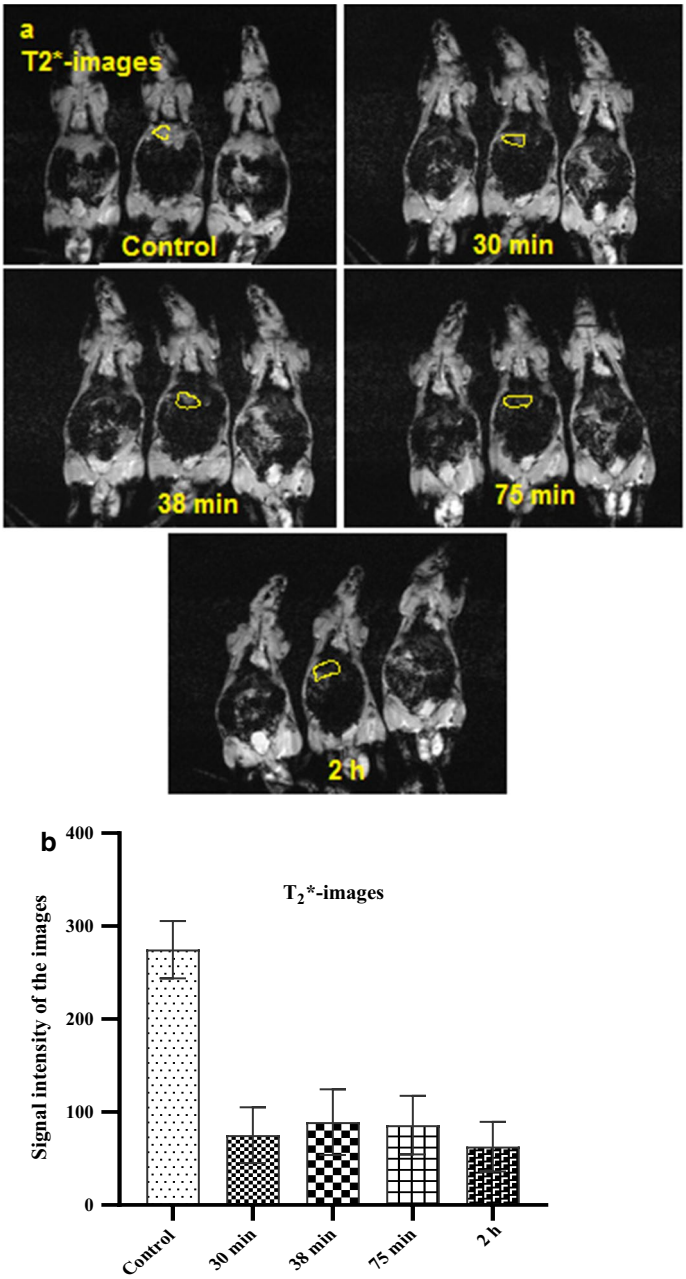


**Fig. 7** **a** *T*2* weighted MRI of the rat liver injected with DMSA-coated Zn-Co NPs; (**b**) signal intensity analysis for *T*2* weighted MR images at different time

Metallic NPs, such as iron, nickel, cobalt, and their alloys, have higher magnetization values than that of oxide NPs [27]. For this reason, in this study, Co–Zn ferrite magnetic NPs were used for further investigation. In a study by Barcena et al. [28], the researchers reported that zinc ferrite NPs increase the $1/T_2$ relaxivity and improve the sensitivity of MR imaging detection.

Choosing an appropriate NP surface coating for the desired application is important and complex [20]. In this regard, there is a controversy about cell viability. Pisanic et al. [11] demonstrated that DMSA-coated NPs are toxic to neurons; however, in another study, Wilhelm et al. [12] reported that DMSA-coated NPs were non-toxic to HeLa cells. Shahbazi-Gahrouei et al. [22] demonstrated that 14 nm Co–Zn ferrite NPs have not produced any toxicity in PC3 human prostate cancer cells. An increase in the concentration of DMSA-coated NPs led to a proliferation of this cell line. Also, these results were confirmed by those of Ge et al. [25]. The mechanisms related to a proliferation of cancer cells and toxicity induction are unknown and need more research. Alternatively, Sattarahmady et al. [21] synthesized dextrin-coated zinc-doped $Zn_{0.5}Co_{0.5}Fe_2O_4$NPs with relaxivity ($r_2$ and $r_2$*) values of 8.5 and 79 mmol $L^{-1}$ $s^{-1}$, respectively. Tumor-bearing C57 mice were used for in vivo MR imaging and the NPs induced negative contrast enhancement in the regions of the tumor. They found 12.5% and 66.5% contrast enhancement for $T_2$- and $T_2^*$-weighted images, respectively, after NP injection, and this enhancement in our study was 58.46% and 77.13% showing a good agreement especially in $T_2^*$-weighted images.

Cobalt ferrite NPs were studied as a contrast agent in MR imaging by Vecchione et al. [29] using lecithin-stabilized nanoemulsions loaded with $Co_{0.5}Fe_{2.5}O_4$ nanocubes. The contrast enhancement was found to be dependent on the nanoemulsion concentration. Melanoma-bearing C57BL/6 male mice were used for in vivo imaging, and after intravenous injection, a time-dependent accumulation was found in the tumor parenchyma. In the current study, we also found this relationship between the contrast enhancement and NP concentration.

Zhang et al. [30] synthesized tetramethylrhodamine (TAMRA)-labeled poly (isobutylene-maleic anhydride) TAMRA-coated $CoFe_2O_4$@$MnFe_2O_4$ NPs for combined MR imaging and fluorescent labeling in vitro using MGC-803 human gastric cell line and in vivo using MGC-803 tumor-bearing female BALB/c mice. They reported that NPs can increase the contrast enhancement in MR imaging at the tumor site so that the highest variation in $T_2$-weighted value was observed at 12 h post injection. However, this number was observed about 30 min after injection in our study, in addition, the greatest contrast enhancement for $T_2$*-weighted images, among the selected times, was 2 h after injection.

The relaxation rate has an inverse relationship with NP size, magnetic moment, and concentration [31]. Jun et al. [32] reported that the values of magnetization saturation are dependent on the size and composition of NPs. The ferrite NPs' size should be small enough to have maximized magnetization and large enough without compromising magnetization or losing superparamagnetivity. As the $T_2$-negative contrast enhancers, ferrite NPs may also act as $T_1$ contrast enhancers after NP cellular breakdown in vivo as Fe (III) which is strongly paramagnetic [32]. In vivo toxicity of zinc-doped ferrite nanoparticle-based contrast agents is

much lower compared to gadolinium-based contrast agents where toxicity is a major issue.

The effectiveness of DMSA-coated Co–Zn ferrite NPs as MRI contrast agents has been evaluated in several studies [16, 33]. In an in vitro study by Ghasemian et al. [16], Co–Zn ferrite NPs ($Co_{0.5}Zn_{0.5}Fe_2O_4$) with and without DMSA coating were investigated on human prostate cancer cell lines (DU145 and PC3) as contrast MR imaging agents. They reported that bare and coated MNPs are suitable as $T_2$-weighted MR imaging contrast agents. Also, $r_2$ value was 28.8 mmol $L^{-1}$ $s^{-1}$ for coated MNPs which is in line with our result (32.85 mmol $L^{-1}$ $s^{-1}$).

We studied the rat liver to evaluate the effectiveness of synthesized NPs as MRI contrast agents. The liver organ was chosen because the previous studies reported that the liver could be a suitable organ for indicating the contrast agent's effectiveness on enhancing image contrast [18, 34]; however, it is possible to assess the contrast enhancement for other sites and organs, and also the study can be carried out at different times to obtain the best time enhancement. Other alternative NPs' surface-coating materials could also serve as a future research subject.

## 5 Conclusion

Microscopic studies of synthesized DMSA-coated Co–Zn ferrite NPs have revealed that the shape of these NPs is spherical with $8 \pm 1$ nm diameter. For these NPs, a saturation magnetization $r_2$ and $r_2$* values were obtained equal to 32.85 and 168.96 mmol $L^{-1}$ $s^{-1}$, respectively, indicating that these NPs are suitable contrast agents for both $T_2$- and $T_2$*-weighted MRI. In vivo study on rat liver showed that the constructed NPs are appropriate novel contrast agents for MR imaging.

**Acknowledgments** This article was extracted from a master's thesis in Medical Physics by the first author and it was supported by Shiraz University of Medical Sciences (grant number: 8833 and ethical committee consent number: IR.SUMS.REC.1394.S919). The authors would like to thank the center of Comparative and Experimental Medicine at Shiraz University of Medical Sciences, and the MRI center of Faghihi Hospital (Shiraz, Iran).

### Compliance with ethical standards

**Conflict of interest** Author declared that there is no conflict of interest for all authors.

## References

1. M. Colombo, S. Carregal-Romero, M.F. Casula, L. Gutiérrez, M.P. Morales, I.B. Böhm, J.T. Heverhagen, D. Prosperi, W.J. Parak, Chem. Soc. Rev. **41**(11), 4306–4334 (2012)
2. R. Ghosh Chaudhuri, S. Paria, Chem. Rev. **112**(4), 2373–2433 (2012)
3. B. Issa, I.M. Obaidat, B.A. Albiss, Y. Haik, Int J Mol. Sci. **14**(11), 21266–21305 (2013)
4. D.K. Mishra, V. Sathe, J. Phys. Condens. Matter. **23**(7), 072203 (2011)
5. B. Nakhjavan, M.N. Tahir, M. Panthöfer, H. Gao, T.D. Schladt, T. Gasi, V. Ksenofontov, R. Branscheid, S. Weber, U. Kolb, L.M. Schreiber, W. Tremel, J. Mater. Chem. **21**(19), 6909–6915 (2011)
6. R. Skomski, (2003) J. Phys. Condens. Matter **15**, R841–R896
7. L. Shen, Y. Qiao, Y. Guo, S. Meng, G. Yang, M. Wu, J. Zhao, Ceram. Int. **40**(1), 1519–1524 (2014)

8. G.-L. Davies, I. Kramberger, J.J. Davis, Chem. Commun. **49**(84), 9704–9721 (2013)
9. A. Goldman, Modern Ferrite Technol. **1**, 395–402 (2006)
10. E. Kneller, F. Luborsky, J. Appl. Phys. **34**(3), 656–658 (1963)
11. T.R. Pisanic II, J.D. Blackwell, V.I. Shubayev, R.R. Fiñones, S. Jin, Biomaterials **28**(16), 2572–2581 (2007)
12. C. Wilhelm, C. Billotey, J. Roger, J. Pons, J.-C. Bacri, F. Gazeau, Biomaterials **24**(6), 1001–1011 (2003)
13. I. Sharifi, H. Shokrollahi, M.M. Doroodmand, R. Safi, J. Magn. Magn. Mater. **324**(10), 1854–1861 (2012)
14. A. Laschewsky, Curr. Opin. Colloid. Interface. Sci. **8**(3), 274–281 (2003)
15. S.Y. Srinivasan, K.M. Paknikar, D. Bodas, V. Gajbhiye, Nanomedicine **13**(10), 1221–1238 (2018)
16. Z. Ghasemian, D. Shahbazi-Gahrouei, S. Manouchehri, Avicenna J. Med. Biotechnol. **7**(2), 64 (2015)
17. L. Li, W. Jiang, K. Luo, H. Song, F. Lan, Y. Wu et al., Theranostics **3**(8), 595 (2013)
18. P. Kennedy, B. Taouli, Nat. Rev. Gastroenterol. Hepatol. **1**, 2 (2020)
19. S. Singhal, R. Sharma, T. Namgyal, S. Jauhar, S. Bhukal, J. Kaur, Ceramics Internat **38**(4), 2773–2778 (2012)
20. M. Latorre, C. Rinaldi, Puerto. Rico. Health. Sci. J. **28**, 3 (2009)
21. N. Sattarahmady, T. Zare, A. Mehdizadeh, N. Azarpira, M. Heidari, M. Loti, H. Heli, Colloids Surf. B **129**, 15–20 (2015)
22. D. Shahbazi-Gahrouei, Z. Ghasemian, M. Abdolahi, S. Manouchehri, S. Javanmard, N. Dana, J. Mol. Biomark Diagn. **4**(3), 154 (2013)
23. I. Sharifi, A. Zamanian, A. Behnamghader, J. Ultra. Grain. Nanostruct. Mater. **49**(2), 87–91 (2016)
24. M.S. Darwish, H. Kim, H. Lee, C. Ryu, J.Y. Lee, J. Yoon, Nanomaterials **9**(8), 1176 (2019)
25. G. Ge, H. Wu, F. Xiong, Y. Zhang, Z. Guo, Z. Bian, J. Xu, C. Gu, N. Gu, X. Chen, D. Yang, Nanoscale. Res. Lett. **8**(1), 1–10 (2013)
26. T. Lam, P. Pouliot, P.K. Avti, F. Lesage, A.K. Kakkar, Adv. Coll. Interface Sci. **199**, 95–113 (2013)
27. W.S. Seo, J.H. Lee, X. Sun, Y. Suzuki, D. Mann, Z. Liu, M. Terashima, P.C. Yang, M.V. McConnell, D.G. Nishimura, H. Dai, Nat. Mater. **5**(12), 971–976 (2006)
28. M. Corti, A. Lascialfari, E. Micotti, A. Castellano, M. Donativi, A. Quarta, P.D. Cozzoli, L. Manna, T. Pellegrino, C. Sangregorio, J. Magn. Magn. Mater. **320**(14), e320–e323 (2008)
29. R. Vecchione, V. Quagliariello, P. Giustetto, D. Calabria, A. Sathya, R. Marotta, M. Profeta, S. Nitti, N. Silvestri, T. Pellegrino, R.V. Iaffaioli, P.A. Netti, Nanomed. NanotechnolBiol. Med. **13**(1), 275–286 (2017)
30. Q. Zhang, T. Yin, G. Gao, J.G. Shapter, W. Lai, P. Huang, W. Qi, J. Song, D. Cui, ACS Appl. Mater. Interfaces **9**(21), 17777–17785 (2017)
31. R. Chaudhary, R. Kanwar, J. Kanwar, J. Nanomater Mol. Nanotechnol. **4**, 3 (2015)
32. Y-w Jun, Y.-M. Huh, J.-S. Choi, J.-H. Lee, H.-T. Song, S. Kim, S. Yoon, K.S. Kim, J.S. Shin, J.S. Suh, J. Cheon, J. Am. Chem. Soc. **127**(16), 5732–5733 (2005)
33. D. Jnaneshwara, D. Avadhani, B.D. Prasad, B. Nagabhushana, H. Nagabhushana, S. Sharma, S.C. Prashantha, C. Shivakumara, J. Alloy. Compd. **587**, 50–58 (2014)
34. N.N. Paranawithana, A.F. Martins, V. Clavijo Jordan, P. Zhao, S. Chirayil, G. Meloni, A. Dean Sherry, J. Am. Chem. Soc. **141**(28), 11009–11018 (2019)

## Affiliations

**Leyla Ansari[1] · Ibrahim Sharifi[2] · Hadis Ghadrijan[3] · Negar Azarpira[4,5] · Farideh Momeni[1] · Hamed Zamani[6] · Naser Rasouli[3] · Mahdi Mohammadi[7] · Alireza Mehdizadeh[1,8] · Razzagh Abedi-Firouzjah[9]**

1 Department of Medical Physics and Medical Engineering, School of Medicine, Shiraz University of Medical Sciences, Shiraz, Iran

2 Department of Material Engineering, Faculty of Engineering, Shahrekord University, Shahrekord, Iran

3 Department of Medical Physics, Isfahan University of Medical Sciences, Isfahan, Iran

4 Transplant Research Center, Shiraz University of Medical Sciences, Shiraz, Iran

5 Nanomedicine and Nanobiology Research Center, Shiraz University of Medical Sciences, Shiraz, Iran

6 Department of Medical Physics, Faculty of Medicine, Shahid Sadoughi University of Medical Sciences, Yazd, Iran

7 Department of Medical Physics and Biomedical Engineering, School of Medicine, Tehran University of Medical Sciences, Tehran, Iran

8 Research Center for Neuromodulation and Pain, Shiraz University of Medical Sciences, Shiraz, Iran

9 Cellular and Molecular Research Center, Yasuj University of Medical Sciences, Yasuj, Iran